Article

Journal of the Brazilian Chemical Society

https://dx.doi.org/10.21577/0103-5053.20240188

*J. Braz. Chem. Soc.* **2025**, *36*, 4, e-20240188, 1-12


# Naphthoxazoles Derived from Lapachol as Fluorescent DNA Probes: Synthesis and Binding Studies with Calf Thymus DNA

***Délis G. Guimarães,[a] Victória L. A. Santos,[a] Sidney S. Simplicio,[b] Arlan A. Gonsalves,[b] João J. S. Gouveia,[c] Fernanda B. Almeida,[d] Luiza A. Gusmão,[e] Antonio C. Tedesco,[e] Fernando L. Primo,[d] Larissa A. Rolim[a] and Cleônia R. M. Araújo*** *[,f]

[a]*Colegiado de Biotecnologia-Rede Nordeste de Biotecnologia (RENORBIO), Universidade Federal Rural de Pernambuco, 52171-900 Recife-PE, Brazil*

[b]*Colegiado de Pós-Graduação Ciências dos Materiais, Universidade Federal do Vale do São Francisco, 56304-917 Petrolina-PE, Brazil*

[c]*Colegiado de Pós-Graduação Ciências Veterinárias no Semiárido, Universidade Federal do Vale do São Francisco, 56304-917 Petrolina-PE, Brazil*

[d]*Departamento de Engenharia de Bioprocessos e Biotecnologia, Faculdade de Ciências Farmacêuticas, Universidade Estadual Paulista, 14800-903 Araraquara-SP, Brazil*

[e]*Departamento de Química, Faculdade de Filosofia Ciências e Letras de Ribeirão Preto, Universidade de São Paulo, 14040-901 Ribeirão Preto-SP, Brazil*

[f]*Colegiado de Pós-Graduação Ciências da Saúde e Biológicas, Universidade Federal do Vale do São Francisco, 56304-917 Petrolina-PE, Brazil*

This study evaluated the potential of naphthoxazoles derived from lapachol as fluorescent deoxyribonucleic acid (DNA) probes. We synthesized three 2-substituted naphthoxazoles: one with a phenyl group (**LOX1**), and two with 2-hydroxyphenyl (**LOX2**) and 4-fluorophenyl (**LOX3**) groups, respectively. The compounds were synthesized using the Debus-Radziszewski reaction between the lapachol and aldehydes. The quantum yield ($\Phi_f$) was determined using the classical relative method with 4',6-diamidino-2-phenylindole (DAPI) as the standard, and the fluorescence lifetime ($\tau_f$) was measured with a lifetime fluorescence spectrometer. The naphthoxazoles exhibited low fluorescence emission and consequently low values of $\Phi_f$ in their free form, demonstrating behavior similar to that of DAPI. These compounds displayed notably large Stokes shifts (approximately 340 nm) and the $\tau_f$ in the nanosecond range. DNA binding studies were conducted by monitoring changes in the absorption properties of naphthoxazoles in the absence and presence of calf thymus DNA at different concentrations. The results indicated that naphthoxazoles interacted with DNA through groove binding. **LOX2** exhibited a binding constant ($K_b$) of $2.70 \times 10^4$ $M^{-1}$, indicating strong binding to the biomolecule. These findings underscore the potential of **LOX1**, **LOX2**, and **LOX3** as candidates for use as fluorescent DNA probes.

**Keywords:** natural naphthoquinone, oxazole, DNA dye, groove binder, fluorescent marker

## Introduction

Naphthoxazoles are fluorophores exhibiting promising photophysical characteristics, such as UV-Vis absorption and fluorescence emission, large Stokes shifts, increased fluorescence upon binding to biological targets, and high photostability.[1-4] Naphthoxazole derivatives result from substituting the oxazole ring at positions 4 and 5 with the naphthalene ring.[5] These compounds can be obtained with high yields through one-pot synthesis protocols.[1,5]

Fluorescent probes are extensively employed for deoxyribonucleic acid (DNA) studies.[6,7] However, commonly used fluorescent DNA probes may be potentially toxic.[8-10] Therefore, non-toxic and biocompatible organic fluorophores, with adjustable optical properties depending

*e-mail: cleonia.araujo@univasf.edu.br
Editor handled this article: Fernando C. Giacomelli (Associate)

on the microenvironment, are valuable tools for probing interactions with DNA.[11]

The literature[5,12,13] reported the naphthoxazoles low toxicity; fluorophores derived from this class of compounds represent a sensitive and safe alternative to commercially available DNA fluorescent probes.

In this article, we present the synthesis, structural and photophysical characterization, and DNA interaction study of new naphthoxazole derivatives prepared from lapachol. We designed three 2-substituted naphthoxazoles derived from lapachol: one with a phenyl group (**LOX1**), and two with the 2-hydroxyphenyl (**LOX2**) and 4-fluorophenyl (**LOX3**) groups, respectively (Scheme 1).

## Experimental

### General

In the synthesis experiments, reagents were purchased from Sigma-Aldrich (St. Louis, MO, USA) and used without preliminary purification, except lapachol, which was extracted from the wood of the yellow ipê (*Tabebuia* sp.). Thin-layer chromatography (TLC) (silica gel on aluminum chromatofoils with fluorescent indicator 254 nm) was purchased from Sigma-Aldrich (St. Louis, MO, USA) and was used to monitor the reaction progress. Column chromatography purification was carried out using silica gel pore size 60 Å, 230-400 mesh particle size were purchased from Sigma-Aldrich (St. Louis, MO, USA).

DNA sodium salt from calf thymus (CT-DNA type I, fibers form; Sigma-Aldrich, St. Louis, MO, USA) was employed in studies of interaction with the naphthoxazoles derivatives evaluated. A stock solution of CT-DNA was prepared by dissolving an appropriate amount of tris(hydroxymethylaminomethane)-HCl buffer (0.1 M, pH 7.4) and stored at 4 °C. The concentration of the stock solution of CT-DNA was determined by UV-Vis analysis using the Beer-Lambert equation with a molar absorptivity (ε) value of 6600 $M^{-1}$. To evaluate the purity of DNA against protein contamination, we used the ratio of absorbance at 260 and 280 nm ($A_{260}/A_{280}$); a value between 1.8 and 1.9 indicates that the DNA is protein-free.[3,14,15]

### Instrumentation

All compounds were characterized by $^{1}H$ and $^{13}C$ nuclear magnetic resonance (NMR) spectroscopy, infrared (IR) spectroscopy, and high-resolution mass spectrometry (HRMS). $^{1}H$ NMR and $^{13}C$ NMR spectra were recorded on a Bruker Ascend™ spectrometer (Zurich, Switzerland) (400 MHz for $^{1}H$ and 100 MHz for $^{13}C$) in deuterated dimethyl sulfoxide (DMSO-$d_6$). The chemical shifts ($\delta$) were reported in parts *per* million (ppm) and are referenced to either the residual solvent peak or tetramethylsilane (TMS) when possible. Coupling constants ($J$) were measured in hertz (Hz). Peaks are denoted as s (singlet), d (doublet), t (triplet) and m (multiplet). Fourier transform infrared (FTIR) spectra were acquired using the IRTracer-100 equipment (Shimadzu, Tokyo, Japan) with KBr pellets as the solid support. Scan were performed in the range of 4000 to 400 $cm^{-1}$ with a resolution of 8 $cm^{-1}$ and 45 scans. High-resolution mass spectrometry (HRMS) was obtained using a Q-TOF (ESI-Q-TOF) mass spectrometer (Waters Synapt XS, Wilmslow, United Kingdom).

Absorption spectra were recorded using a Shimadzu UV-2600 absorption spectrometer (Tokyo, Japan) with 1.0 cm optical path length and covering the 200-800 nm region.

To determine the fluorescence quantum yield, samples were first evaluated using a UV-Vis spectrophotometer (Genesys 10S, Thermo Fisher Scientific, Madison, USA) within the 190-500 nm range, using a quartz cuvette to measure the maximum absorption wavelength with an absorbance below 0.1. The samples were then analyzed with a RF-6000 spectrofluorometer (Shimadzu Corporation, Nakagyo-ku, Kyoto, Japan), with excitation fixed at 345 nm and emission measured in the range of 640-800 nm, using slit opening of 10 nm for both excitation and emission, respectively.

To determine the fluorescence lifetime of the **LOX1**, **LOX2**, and **LOX3** samples, a lifetime fluorescence

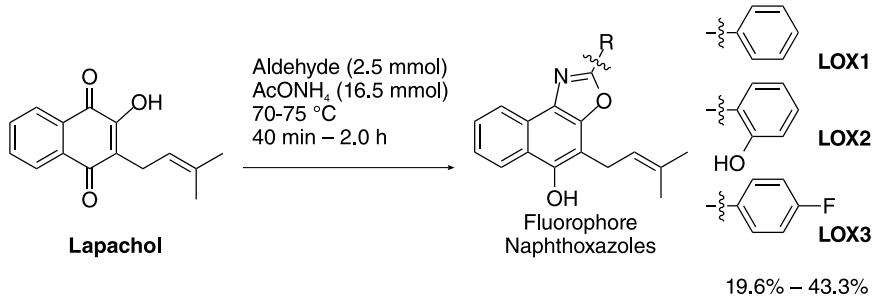


**Scheme 1.** Synthesis reaction naphthoxazoles (**LOX1**, **LOX2**, and **LOX3**).

spectrometer (EasyLife X, HORIBA Scientific, Sofia, Bulgaria) equipped with light emitting diode (LED) with excitation at 375 nm was used, following the protocol described in the equipment manual. All samples were prepared in DMSO.

## Synthesis

### Extraction and purification of lapachol

Lapachol was extracted from the heartwood of a *Tabebuia* genus and purified through recrystallization using ethanol.[16] The heartwood of *Tabebuia* sp. was removed and cut into small, thin pieces (50 g). These pieces were then placed in 400 mL of a 1% (m/v) NaOH solution and left to stand for 24 h. The mixture was filtered, and the resulting dark red solution was acidified by slowly adding a 6.0 M HCl solution until a yellow solid precipitated. The solid was filtered and purified by recrystallization in hot ethanol. Lapachol was obtained as yellow crystals with a yield of 3.5% (m/m); melting point (mp) 138.3-140.3 °C.

### General synthesis of the naphthoxazoles derived from lapachol (**LOX1**, **LOX2**, and **LOX3**)

The access was registered in the National System of Genetic Heritage and Associated Traditional Knowledge (SisGen) under the A5FDA89. A yellow solid was obtained with a yield of 1.5% (m/m) and mp 138.3-140.3 °C (lit.[16] mp 138.3-140.3 °C).

To a solution of lapachol (1 mmol) in ethanol (6 mL), the appropriate aromatic aldehyde (2.5 mmol of benzaldehyde, salicylaldehyde, or 4-fluorobenzaldehyde) was added, and the mixture was heated in a glycerin bath at 70-75 °C; at this point, ammonium acetate (16.5 mmol) was added. The reaction was conducted in a closed system with a gas conditioning setup attached to the reaction flask. After the total consumption of lapachol, the reaction mixture was treated with 5% (m/v) sodium bisulfite solution at approximately 0 °C.[16-18]

### 4-(3-Methylbut-2-enyl)-2-phenylnaphtho[1,2-*d*]oxazol-5-ol (**LOX1**)

The complete consumption of lapachol occurred 2 h after the reaction started. After treatment with a sodium bisulfite solution, the reaction mixture produced a precipitate, which was purified by column chromatography. A white solid was obtained with a yield of 19.6% and a mp 165-167 °C (lit.[17] mp 168 °C); $^1$H NMR (400 MHz, DMSO-$d_6$) $\delta$ 9.67 (s, 1H), 8.36 (m, 2H), 8.21 (m, 2H), 7.62 (m, 5H), 5.42 (m, 1H), 3.80 (d, 2H, *J* 7.3 Hz), 1.92 (s, 3H), 1.68 (s, 3H); $^{13}$C NMR (100 MHz, DMSO-$d_6$) $\delta$ 159.94 (C), 148.22 (C), 131.81 (C), 130.89 (CH), 129.66 (C), 129.31 (CH), 127.08 (C), 126.71 (CH), 126.32 (CH), 124.60 (CH), 124.36 (C), 124.19 (C), 123.39 (CH), 121.56 (CH), 121.39 (CH), 109.28 (C), 25.49 ($CH_3$), 23.35 ($CH_2$), 17.83 ($CH_3$); IR (KBr) $\nu$ / cm$^{-1}$ 3194 (O–H), 1639 (C=N), 1172 (C–O); HRMS (ESI) *m/z*, calcd. for $C_{22}H_{19}NO_2$: 329.1416, found: 330.1518 $[M + H]^+$.

### 2-(2-Hydroxyphenyl)-4-(3-methylbut-2-enyl)naphtho[1,2-*d*]oxazol-5-ol (**LOX2**)

After 40 min from the start of the reaction, the product precipitated. The solid was filtered and washed with ethanol and sodium bisulfite solution. A white solid was obtained with a yield of 43.3% and mp 191-194 °C; $^1$H NMR (400 MHz, DMSO-$d_6$) $\delta$ 11.25 (s, 1H), 9.78 (s, 1H), 8.37 (t, 2H, *J* 8.6 Hz), 8.01 (d, 1H, *J* 7.5 Hz), 7.67 (t, 1H, *J* 7.4 Hz), 7.58 (t, 1H, *J* 7.5 Hz), 7.49 (t, 1H, *J* 7.6 Hz), 7.13 (m, 2H), 5.41 (t, 1H, *J* 6.5 Hz), 3.80 (d, 2H, *J* 7.1 Hz), 1.92 (s, 3H), 1.68 (s, 3H); $^{13}$C NMR (100 MHz, DMSO-$d_6$) $\delta$ 159.73 (C), 156.74 (C), 148.64 (C), 146.87 (C), 132.82 (CH), 131.95 (C), 127.56 (C), 126.94 (CH), 126.44 (CH), 124.90 (CH), 124.22 (C), 123.46 (C), 123.40 (CH), 121.52 (CH), 121.42 (CH), 119.97 (CH), 117.08 (CH), 110.97 (C), 109.15 (C), 25.50 ($CH_3$), 23.29 ($CH_2$), 17.83 ($CH_3$); IR (KBr) $\nu$ / cm$^{-1}$ 3429 (O–H), 1627 (C=N), 1195 (C–O); HRMS (ESI) *m/z*, calcd. for $C_{22}H_{19}NO_3$: 345.1365, found: 346.1472 $[M + H]^+$.

### 2-(4-Fluorophenyl)-4-(3-methylbut-2-enyl)naphtho[1,2-d]oxazol-5-ol (**LOX3**)

The complete total consumption of lapachol occurred 1 h and 20 min after the onset of the reaction. After treatment with sodium bisulfite solution, the reaction mixture yielded a precipitate that was purified by column chromatography. A white solid was obtained with a yield of 20.4% and mp 158-159 °C; $^1$H NMR (400 MHz, DMSO-$d_6$) $\delta$ 9.66 (s, 1H), 8.34 (d, 2H, *J* 9.1 Hz), 8.23 (m, 2H), 7.65 (t, 1H, *J* 7.8 Hz), 7.56 (m, 1H), 7.47 (m, 2H), 5.41 (m, 1H), 3.78 (d, 2H, *J* 7.3 Hz), 1.91 (s, 3H), 1.68 (s, 3H); $^{13}$C NMR (100 MHz, DMSO-$d_6$) $\delta$ 163.58 (d, $^1J$ ($^{19}$F, $^{13}$C) 249.2 Hz, C4'), 159.15 (C), 148.24 (C), 148.21 (C), 131.81 (C), 129.62 (C), 128.79 (d, $^3J$ ($^{19}$F, $^{13}$C) 8.9 Hz, C2' and C6'), 126.70 (CH), 124.61 (CH), 124.33 (C), 124.18 (C), 123.75 (d, $^4J$ ($^{19}$F, $^{13}$C) 2.8 Hz, C1'), 123.38 (CH), 121.55 (CH), 121.37 (CH), 116.49 (d, $^2J$ ($^{19}$F, $^{13}$C) 22.3 Hz, C3' and C5'), 109.27 (C), 25.48 ($CH_3$), 23.33 ($CH_2$), 17.82 ($CH_3$); IR (KBr) $\nu$ / cm$^{-1}$ 3352 (O–H), 1608 (C=N), 1230 (C–F), 1153 (C–O); HRMS (ESI) *m/z*, calcd. for $C_{22}H_{18}FNO_2$: 347.1322, found: 348.1426 $[M + H]^+$.

### Fluorescence quantum yields (Φf) determination

The fluorescence quantum yield ($\Phi_f$) ($\lambda_{exc}$ = 345 nm) of the **LOX1**, **LOX2**, and **LOX3** samples was determined

using the methodology described by Zhang *et al.*,[19] which is based on the classical relative method. All samples were prepared in DMSO, while the 4',6-diamidino-2-phenylindole (DAPI) standard ($\Phi_f = 0.021$), was prepared in water, as previously described by Prajapati *et al.*[20] The fluorescence quantum yields were then calculated using equation 1:

$$\Phi_f = \Phi_f^r \times \frac{F_s}{F_0} \times \frac{A_0}{A_s} \times \frac{n_s^2}{n_0^2} \quad (1)$$

where, $\Phi_f$ denotes the fluorescence quantum yield, F represents the integrated fluorescence intensity, A signifies the absorbance at the excitation wavelength and n indicates the refractive index of the solvent used. The subscript 0 refers to the reference, and the subscript s refers to the sample.

### DNA binding study by UV-Vis absorption analysis

Absorption spectra of **LOX1**, **LOX2**, and **LOX3** both in the absence of and in the presence of increasing concentrations of CT-DNA were obtained at room temperature in DMSO (5%)/Tris-HCl buffer (0.1 M, pH 7.4) mixture solution in the 200-800 nm range, and DMSO (5%)/Tris-HCl buffer (0.1 M, pH 7.4) was used as a reference medium. The concentrations naphthoxazoles were fixed at 10 μM, while CT-DNA concentrations varied from 0 to 320 μM. The naphthoxazole-DNA solutions were allowed to equilibrate at room temperature for 5 min before absorption spectra were recorded. The spectra were acquired using a rectangular quartz cuvette with a 1 cm optical path length. The percentage of hypochromism or hyperchromism (H) was calculated using the equation $H\ (\%) = (A_{free} - A_{bound})/A_{free} \times 100$, where $A_{free}$ is the absorbance before interaction with DNA, and $A_{bound}$ is the absorbance after interaction with DNA. Bathochromic or hypsochromic shift was quantified by the equation $\Delta\lambda = \lambda_{final} - \lambda_{initial}$, $\lambda_{initial}$ is the wavelength of maximum absorption before interaction with DNA, and $\lambda_{final}$ is the wavelength of maximum absorption after interaction with DNA.[2,21] Data analysis and calculations were performed using Microsoft Excel (Microsoft Corporation, Redmond, WA, USA).[22]

## Results and Discussion

### Synthesis and structural characterization

The naphthoxazoles (**LOX1**, **LOX2**, and **LOX3**) were synthesized using the Debus-Radziszewski reaction in a one-pot process involving lapachol and the corresponding aldehyde, with ammonium acetate serving as the source of ammonia (Scheme 1).[16-18]

The Debus-Radziszewski reaction typically employs an α-dicarbonyl compound, an aldehyde, and a nitrogen source. This reaction is one of the most commonly used methodologies for obtaining 2,4,5-substituted imidazoles. However, subsequent studies have reported that, in some cases, the Debus-Radziszewski methodology allows for the formation of two isosteric azoles: imidazole and oxazole.[5,23]

In this study, the previously mentioned reaction predominantly yielded oxazole derivatives, leading to cleaner reactions. According to Del Rio *et al.*,[18] since lapachol possesses only one free carbonyl group, the formation of an imidazole derivative, a keto-enol tautomerization of its phenolic hydroxyl would be necessary to generate an *o*-quinonimine intermediate. However, this process results in the loss of ring aromaticity,

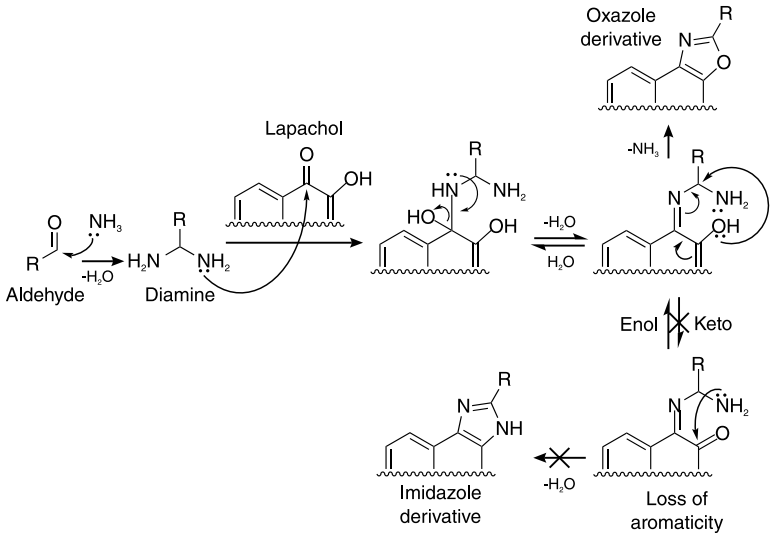


**Figure 1.** Proposed mechanism for the Debus-Radziszewski reaction from lapachol.

which disfavors the formation of the keto tautomer and prevents the nucleophilic attack of the amine. Consequently, the synthetic route to the imidazole is hindered (Figure 1).

The synthetic methodologies used for producing **LOX1**, **LOX2**, and **LOX3** are adaptations, incorporating principles of green chemistry, from previously described methodologies.[16-18] The use of ethanol as the solvent in these reactions not only provides environmental and economic benefits but also results in shorter reaction times (40 min to 2 h) and satisfactory yields (19.6 to 43.3%).

Among the three compounds synthesized in this study, only **LOX1** has been previously described in the literature.[17,18] **LOX2** and **LOX3** represent novel structures. **LOX1**, **LOX2**, and **LOX3** were elucidated through combined analysis of one-dimensional (1D) and two-dimensional (2D) NMR spectra and were confirmed by IR and HRMS techniques.

It is known that the synthesis of naphthoxazoles from lapachol typically yields two derivatives: a minor product, which is naphthoxazole derivative of β-xyloidone, and a major product, which is the naphthoxazole with the isoprenyl side chain of lapachol.[17,18] According to Del Rio *et al*.[18] the formation of the naphthoxazole derivative of β-xyloidone occurs with longer reaction times.

Given the characteristics described in the literature for the naphthoxazolic derivatives of β-xyloidone, we recognize that these compounds may form as secondary products of the reactions. However, due to their low yield and purity, structural analysis was not conducted.

The signals observed in the NMR spectra of **LOX1** are consistent with the literature data for this compound (Table S1, Supplementary Information (SI) section). Additionally, IR and HRMS spectroscopy analyses confirmed the molecular structures of the three naphthoxazoles (**LOX1**, **LOX2**, and **LOX3**) (Figures S13-S16, SI section).

The $^{1}$H NMR spectrum of **LOX2** exhibited a singlet at $\delta_H$ 11.25 ppm (1H). This signal, with a high chemical shift value, is characteristic of the formation of an intramolecular hydrogen bond between the phenolic substituent at position 2 of the oxazole nucleus and its nitrogen,[11] Figure 2 (Figure S1, SI section).

The number of hydrogens obtained from signal integration and their spin-spin coupling corresponds to the structure of **LOX2**. The spectra of the other naphthoxazoles also exhibited integration and multiplicity consistent with their molecular structures.

The $^{13}$C NMR spectrum of **LOX2** (Figure S2, SI section) exhibited 22 peaks corresponding to the carbons present in its molecular structure. The signals at $\delta_C$ 156.74 and 148.64 ppm characterized two oxygenated carbons with sp$^2$ hybridization, corresponding to the carbons of the two hydroxyls of **LOX2**. The signal at $\delta_C$ 148.64 ppm was confirmed as C10 by the heteronuclear 2D $^{1}$H-$^{13}$C heteronuclear multiple bond correlation (HMBC) spectrum (Figure S4, SI section). In this spectrum, the correlation between the signals at $\delta_H$ 8.37 and 3.80 ppm with the carbon C10 ($\delta_C$ 148.64 ppm) was observed. According to the heteronuclear 2D $^{1}$H-$^{13}$C heteronuclear single quantum coherence spectroscopy (HSQC) spectrum (Figure S5, SI section), the signals at $\delta_H$ 8.37 and 3.80 ppm correspond to hydrogens H9 and H12, respectively (Figure 2).

The signal at $\delta_H$ 8.37 ppm (2H) in the homonuclear 2D $^{1}$H-$^{1}$H correlation (COSY) spectrum (Figure S6, SI section), which exhibits coupling between hydrogen atoms, correlates with the signal at $\delta_H$ 7.67 ppm, corresponding to either hydrogen H8 or H7. This suggests that the signal at $\delta_H$ 8.37 ppm corresponds to hydrogen atoms H9 and H6 (Figure 2).

Hydrogen H6 ($\delta_H$ 8.37 ppm), in turn, correlates with the signal at $\delta_C$ 127.56 ppm (C5). Furthermore, the signal at $\delta_H$ 3.80 ppm exhibits a $^{3}J_{H\text{-}C}$ correlation with the signal at $\delta_C$ 146.87 ppm (C4), confirming the presence of the oxazole nucleus in **LOX2** (Figure 2). The chemical shifts of C4 and C5 are similar to those observed by Dias *et al*.[24] for their 2-substituted naphthoxazoles with a phenol group. Figure 2 presents the main chemical shifts and correlations that confirmed the presence of the oxazole nucleus, as discussed earlier.

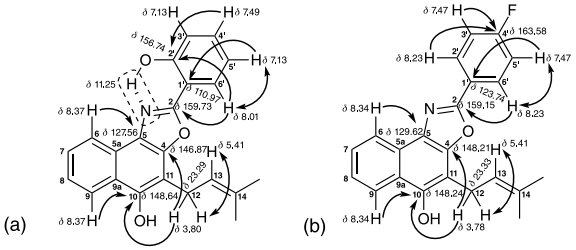


**Figure 2.** Correlations confirming the presence of (a) **LOX2** and (b) **LOX3**. Double arrows represent correlations between vicinal hydrogens observed in the $^{1}$H-$^{1}$H COSY spectrum, while single arrows represent $^{2,3}J_{H\text{-}C}$ correlations through the $^{1}$H-$^{13}$C HMBC spectrum.

Another significant aspect to consider is the chemical shift of carbon C2. As reported by Dias *et al*.,[24] carbon C2 demonstrates chemical shift values ranging from 159.0 to 160.2 ppm. **LOX2** exhibited a chemical shift for C2 of 159.73 ppm. The signal at $\delta_C$ 159.73 ppm displays a $^{3}J_{H\text{-}C}$ correlation with the signal at $\delta_H$ 8.01 ppm. Simultaneously, the signal at $\delta_H$ 8.01 ppm also demonstrates homonuclear correlation with the signal at $\delta_H$ 7.13 ppm (m, 2H) and heteronuclear $^{3}J_{H\text{-}C}$ correlation with the signal at $\delta_C$ 156.74 ppm. Lastly, to confirm the presence of **LOX2**, the signal at $\delta_H$ 7.13 ppm also correlates $^{3}J_{H\text{-}C}$

with the signal at $\delta_C$ 110.97 ppm, which is characteristic of carbon C1' (see Figure 2). The chemical shift value obtained for C1' also corresponds with the values reported by Dias *et al.*[24] (111.4-111.5 ppm for uncoordinated naphthoxazoles).

The structure of **LOX3** was also elucidated through combined analysis of 1D and 2D NMR spectra (Figures S7-S12, SI section). Initially, two characteristic signals of oxygenated carbons with $sp^2$ hybridization were observed at $\delta_C$ 148.24 and 148.21 ppm, corresponding to carbons C10 and C4 of **LOX3**. Although the values might be interchanged due to the similarity of their chemical environment, the chemical shifts of carbons C10 and C4 were confirmed by the $^3J_{H-C}$ correlation between signals at $\delta_H$ 8.34 and 3.78 ppm with both signals at $\delta_C$ 148.24 and 148.21 ppm (Figure 2). The signals at $\delta_H$ 8.34 and 3.78 ppm correspond to hydrogens H9 and H12, respectively. The signal at $\delta_H$ 8.34 ppm (2H), as observed for **LOX2**, corresponds to hydrogens H9 and H6, as confirmed through homonuclear correlations between the signal at $\delta_H$ 8.34 ppm and signals at $\delta_H$ 7.65 and 7.56 ppm corresponding to hydrogens H7 and H8. Hydrogen H6 ($\delta_H$ 8.34 ppm), in turn, correlates with the signal at $\delta_C$ 129.62 ppm (C5), confirming the presence of the oxazole nucleus in **LOX3** (Figure 2). The chemical shifts of C4 and C5 are similar to those reported by Aljaar *et al.*[25] for their 2-substituted naphthoxazole with a fluorobenzene group ($\delta_C$ 148.0 and 137.6 ppm).

Carbon C2 of **LOX3** exhibited a chemical shift value of 159.15 ppm, which is similar to that observed for **LOX2** and characteristic of this carbon in naphthoxazole derivatives, as discussed previously.

Additionally, the signal at $\delta_C$ 159.15 ppm exhibits a $^3J_{H-C}$ correlation with the signal at $\delta_H$ 8.23 ppm. Simultaneously, the signal at $\delta_H$ 8.23 ppm exhibits a homonuclear correlation with the signal at $\delta_H$ 7.47 ppm (m, 2H) and heteronuclear $^3J_{H-C}$ correlation with the signal at $\delta_C$ 163.58 ppm (C4'). Finally, the signal at $\delta_H$ 7.47 ppm also shows a $^3J_{H-C}$ correlation with the signal at $\delta_C$ 123.75 ppm, characteristic of carbon C1', and $^2J_{H-C}$ with the signal at $\delta_C$ 163.58 ppm (Figure 2). The chemical shifts at $\delta_C$ 123.75 and 163.58 ppm for C1' and C4', respectively, are consistent with those reported by Aljaar *et al.*[25] ($\delta_C$ 123.7 and 164.5 ppm).

Furthermore, the $^{13}C$ NMR spectrum of **LOX3** (Figure S8, SI section), also exhibited $^{13}C$-$^{19}F$ couplings, which provided crucial information for the assignment of the previously discussed chemical shifts. According to Pavia *et al.*,[26] when an organic compound has a fluorine atom attached to a carbon-13 atom, a heteronuclear $^{13}C$-$^{19}F$ coupling is observed. As stated by Branco *et al.*,[27] it is more common to obtain $^{13}C$ NMR spectra with $^{13}C$-$^{19}F$ couplings for organofluorides than to obtain decoupled spectra.

In the $^{13}C$ NMR spectrum of **LOX3** (Figure S8, SI section), doublets were observed, reflecting the presence of a fluorine atom in the structure, resulting from $^{13}C$-$^{19}F$ couplings via $^1J_{C-F}$ up to $^4J_{C-F}$. The doublet at $\delta_C$ 163.58 ppm (the value corresponding to the true chemical shift of the carbon atom, at the center of the doublet) corresponds to direct coupling via a bond between the fluorine and C4' (*ipso* carbon) with a high coupling constant, *J* 249.2 Hz. This high coupling constant value is typical in direct fluorine couplings with a carbon-13 atom ($^1J_{C-F}$).[25-27]

Subsequently, the doublet at $\delta_C$ 116.49 ppm, with *J* 22.3 Hz, corresponds to the coupling between the fluorine and the *ortho* carbons, C3' and C5'. As expected, coupling constants decrease with increasing distance between the carbon and the fluorine.[25-27] Meanwhile, the doublet at $\delta_C$ 128.79 ppm, with *J* 8.9 Hz, corresponds to the coupling between the fluorine and the *meta* carbons, C2' and C6'.

Furthermore, the doublet at $\delta_C$ 123.75 ppm, with *J* 2.8 Hz, which corresponds to the coupling between fluorine and carbon C1' via $^4J_{C-F}$, as also reported by Aljaar *et al.*[25] for their 2-substituted naphthoxazole with a fluorobenzene group. It is worth noting that the chemical shift values and coupling constants were all similar to those observed by Aljaar *et al.*,[25] confirming the synthesis of **LOX3**.

### Photophysical properties

The naphthoxazoles are fluorophores that exhibit increased emission intensity upon binding to DNA.[2,3] Therefore, the synthesis of naphthoxazoles with diverse structural characteristics, which could potentially influence their optical properties, should be explored to optimize the efficiency of fluorescent sensors.

**LOX2** is a fluorophore capable of excited-state intramolecular proton transfer (ESIPT), as it features a proton donor group (hydroxyl group –OH) and a proton acceptor group (imine nitrogen –N=) in close proximity, forming an intramolecular hydrogen bond in the ground electronic state (Figure 3).[28,29] On the other hand, **LOX3** is a D-π-A conjugated system, containing an electron donor group (D) separated from an electron acceptor group (A) at the opposite ends other of the molecule by a π-linker bridge.[30,31] Hence, **LOX3** is representative of a class of fluorophores commonly known as push-pull systems (Figure 3).[30,32,33]

In general, fluorophores with these characteristics exhibit large Stokes shifts and sensitivity to polarity, with results in changes to their emission profile in response to environmental conditions, among other properties. These

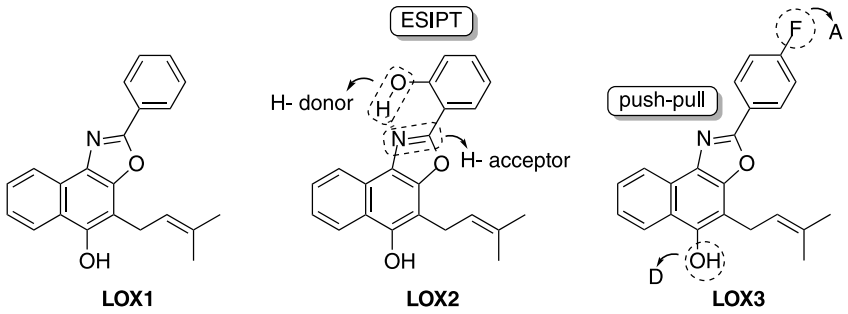


**Figure 3.** Molecular structure of the naphthoxazoles **LOX1**, **LOX2**, and **LOX3**, highlighting the structural features of **LOX2** and **LOX3**.

properties are desirable for fluorescent molecules used in bioimaging.[28,31,33]

Large Stokes shifts eliminate spectral overlap between fluorophore absorption and emission, thereby contributing to a clearer fluorescence signal and reduced background interference.[34-36] The optical characteristics of the naphthoxazoles **LOX1**, **LOX2**, and **LOX3** were studied and are summarized in Table 1. **LOX1**, **LOX2**, and **LOX3** exhibited large Stokes shifts, comparable to DAPI (Table 1). DAPI is a DNA fluorescent probe that binds to the minor groove.[6,37]

**Table 1.** Optical properties of **LOX1**, **LOX2**, and **LOX3** in DMSO, using DAPI in water as the standard, as described by Prajapati *et al.*[20]

| Compound | $\lambda_{abs}^{max}$ / nm | $\lambda_{em}^{max}$ / nm | ΔS / nm ($cm^{-1}$) | $\Phi_f$ | $\tau_f$ / ns |
|---|---|---|---|---|---|
| DAPI | 345 | 693 | 348 (14576) | 0.0210 | 2.78[a] |
| **LOX1** | 348 | 690 | 342 (14242) | 0.0018 | 14.44 |
| **LOX2** | 353 | 690 | 337 (13835) | 0.0020 | 1.45 |
| **LOX3** | 347 | 690 | 343 (14325) | 0.0014 | 8.08 |

[a]Berezin and Achilefu.[38] DAPI: 4',6-diamidino-2-phenylindole; $\lambda_{abs}^{max}$: maximum emission wavelength; ΔS: Stokes shift; $\Phi_f$: fluorescence quantum yield; $\tau_f$: fluorescence lifetime.

Each compound fluorescence quantum yields ($\Phi_f$) were calculated using the classical relative method, with DAPI as the reference standard (Table 1). The $\Phi_f$ is defined as the ratio between the number of photons emitted and the number of photons absorbed by the fluorophore.[19,37,39] The relative method involves evaluating the absorption profile of the molecule followed by fluorescence emission, and then mathematically determining the quantum yield from the data obtained.[19,39]

$\Phi_f$ is a parameter highly sensitive to the concentration of the sample and the excitation wavelength due to the self-absorption effect, wherein the molecule absorbs its own emitted energy.[39] To prevent this effect, the absorbance of the samples should be kept below 0.1 as described by Eaton.[40] Additionally, the chemical environment in which the molecule is solubilized directly impacts the fluorescence emission profile and consequently the fluorescence quantum yield.[37] Substances with a high fluorescence quantum yield, close to 1, exhibit an intense fluorescence emission profile, as nearly all absorbed energy is dissipated as photon emission.[37]

DAPI has a low $\Phi_f$; however, it is well known that this radiative effect increases significantly when bound with DNA molecules.[20] Similarly, we can consider that the **LOX**s behave analogously to DAPI, and exhibit reduced fluorescence in their free form, as demonstrated by the fluorescence quantum yield study (Figure 4).

Fluorescence lifetime ($\tau_f$) refers to the duration for which an electron remains excited before returning to its ground state after absorbing light. During this return to the ground state, the absorbed energy is dissipated through

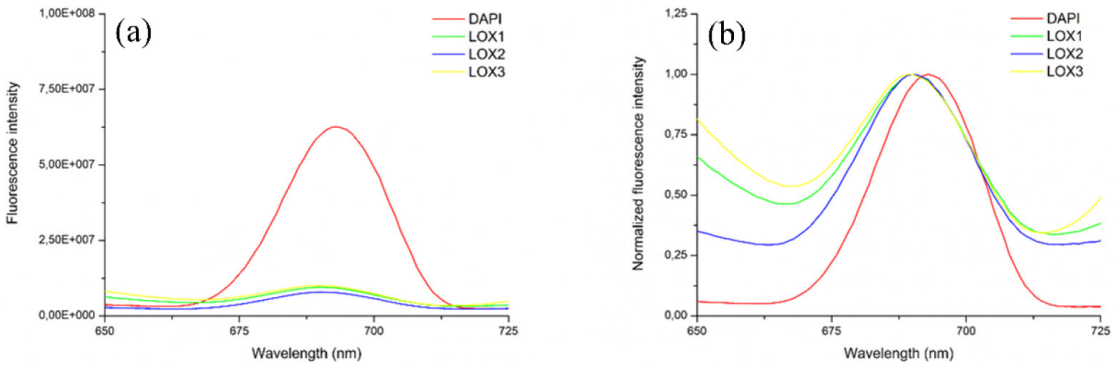


**Figure 4.** UV-Vis 2D fluorescence emission spectra (a) and normalized spectra (b) of **LOX1**, **LOX2**, and **LOX3** in DMSO, with DAPI in water as a standard compound. $\lambda_{exc}$ = 345 nm, with excitation and emission bandwidths of 10 nm each.

fluorescence emission and other non-radiative processes, collectively known as quenching.[37,38]

The $\tau_f$ does not depend on conditions such as the excitation wavelength and the duration of exposure to light. Additionally, it does not depend on fluorescence intensity or fluorophore concentration. As the process of fluorescence emission time is associated with an energetically unstable state, the duration of fluorescence can be sensitive to a wide variety of internal factors such as the structure of the fluorophore, and external factors such as temperature, polarity, and the presence of fluorescence quenchers.[38,41]

In this context, $\tau_f$ can be influenced by reversible changes in electron distribution occurring in the excited state. These changes, which are related to the structure of the fluorophore, are generally less susceptible to environmental factors. Significant processes in this category include excited-state charge transfers, such as electron transfer (ESET) and proton transfer (ESPT), as well as intersystem crossings.[38]

The $\tau_f$ of the **LOX**s in their free state was typically in the nanosecond range, as expected for fluorescent organic dyes.[11,37] Naphthoxazole **LOX2** exhibited the shorter $\tau_f$, at 1.45 ns. This shorter value, in comparison to the naphthoxazoles **LOX1** and **LOX3** (Table 1), suggests the influence of ESIPT on the loss of energy from the excited state, as this process may compete with the radiative process.[38,41] The long lifetimes of **LOX1** and **LOX3** are useful, as long $\tau_f$ are used in biological systems to completely eliminate autofluorescence background.[38]

The increase in $\tau_f$ of fluorophores upon binding to DNA is well-documented. For example, the $\tau_f$ of ethidium bromide (EB) is approximately 1.7 ns in the free form and increases to about 20 ns after binding to DNA.[37,38] This effect results from the restriction of fluorophore mobility upon interaction with DNA, leading to a decrease in non-radiative processes and consequently an increase in $\tau_f$ and fluorescence intensity.[2,38]

## DNA binding study

UV-Vis absorption spectroscopy is the most commonly employed technique for studying DNA interactions with small molecules.[10] This investigation can be conducted by monitoring changes in the absorption properties of either the ligand molecule or the DNA.[10,42,43]

Generally, molecules used as DNA ligands exhibit absorption bands in the visible region, which are easily distinguishable from the absorption bands of DNA. DNA does not absorb in the visible region; its maximum absorption band is in the ultraviolet region at 260 nm.[10,14] Therefore, examining changes in the intensity and position of the absorption bands of the ligand after interaction with DNA, compared to when the ligand molecule is free in solution, can indicate binding between DNA and the molecule.[10,11,14,15,42,44] The extent of this change can be interpreted as an indication of the strength of the interaction between DNA and the ligand.[10,45,46]

Small aromatic molecules can bind to DNA through three main modes of interaction: intercalation between base pairs, binding to minor and major DNA grooves, or electrostatic interactions between phosphate groups and charged species.[10,11]

Compounds that bind to DNA through intercalation typically result in hypochromism and a bathochromic shift (red shift).[2,10,45] In contrast, compounds that interact by binding to the grooves or to phosphate groups often exhibit a hyperchromic effect which may or may not be accompanied by slight bathochromic or hypsochromic shifts (blue shift).[10,47,48] It is important to note that in weak interactions, only hypochromic or hyperchromic effects are observed, that is, without significant changes in the spectral profile.[10,42]

The naphthoxazoles (**LOX1**, **LOX2**, and **LOX3**) exhibited similar absorption profiles in DMSO (5%)/Tris-HCl buffer (pH 7.4) (Figure 5). Each compound displays three main absorption bands of high intensity, the most intense band is in the ultraviolet region, while the remaining bands are in the visible region. The wavelengths of maximum absorption ($\lambda_{abs}$) for **LOX1**, **LOX2**, and **LOX3** are in Figure 5.

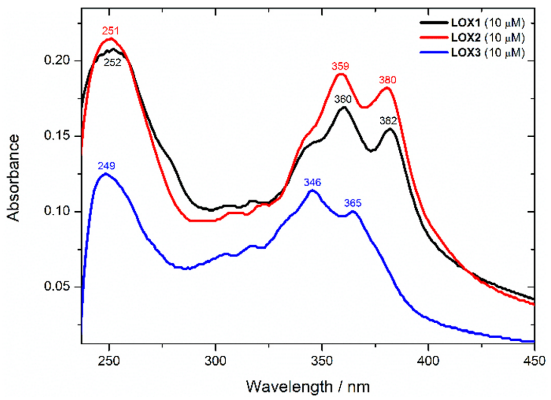


**Figure 5.** UV-Vis absorption spectra of **LOX1**, **LOX2**, and **LOX3** in DMSO (5%)/Tris-HCl buffer (pH 7.4).

Aggregation assays determine the maximum concentration a molecule can reach before it aggregates in solution. The formation of aggregates causes bathochromic or hypsochromic shifts in the absorption spectrum, depending on the type of aggregate.[49,50] The aggregation behavior of **LOX2**, selected as the representative compound, was evaluated using UV-Vis spectroscopy in DMSO(5%)/

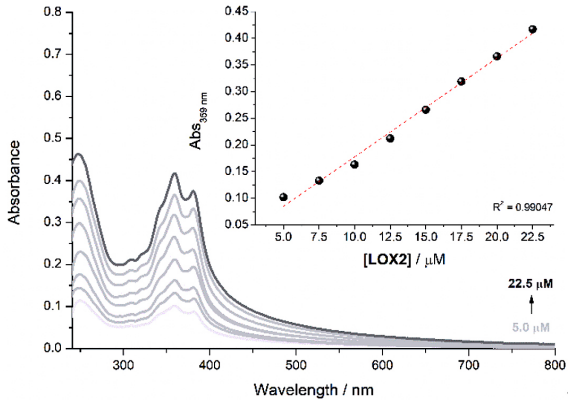


**Figure 6.** Aggregation study of **LOX2** in DMSO (5%)/Tris-HCl buffer (pH 7.4) (inset: plot of the linear relationship of absorbance at 359 nm as a function of the concentration 5.0-22.5 μM).

Tris-HCl buffer (pH 7.4). Aggregation was ruled out as no significant shifts in the maximum absorbance wavelengths were observed. A linear increase in the absorbance was noted as the concentration variation from 5.0 to 22.5 μM (Figure 6).

The naphthoxazoles (**LOX1**, **LOX2**, and **LOX3**) were evaluated for their potential interaction with DNA. DNA binding studies involved monitoring changes in the absorption properties of **LOX1**, **LOX2**, and **LOX3** both in the absence and presence of CT-DNA at various concentrations (Figure 7).

Addition of aliquots of CT-DNA (0-320 μM) to **LOX1** resulted in significant changes to its absorption profile. Initially, a decrease in the absorbance of the main band at 360 nm was observed after the addition of the first aliquots

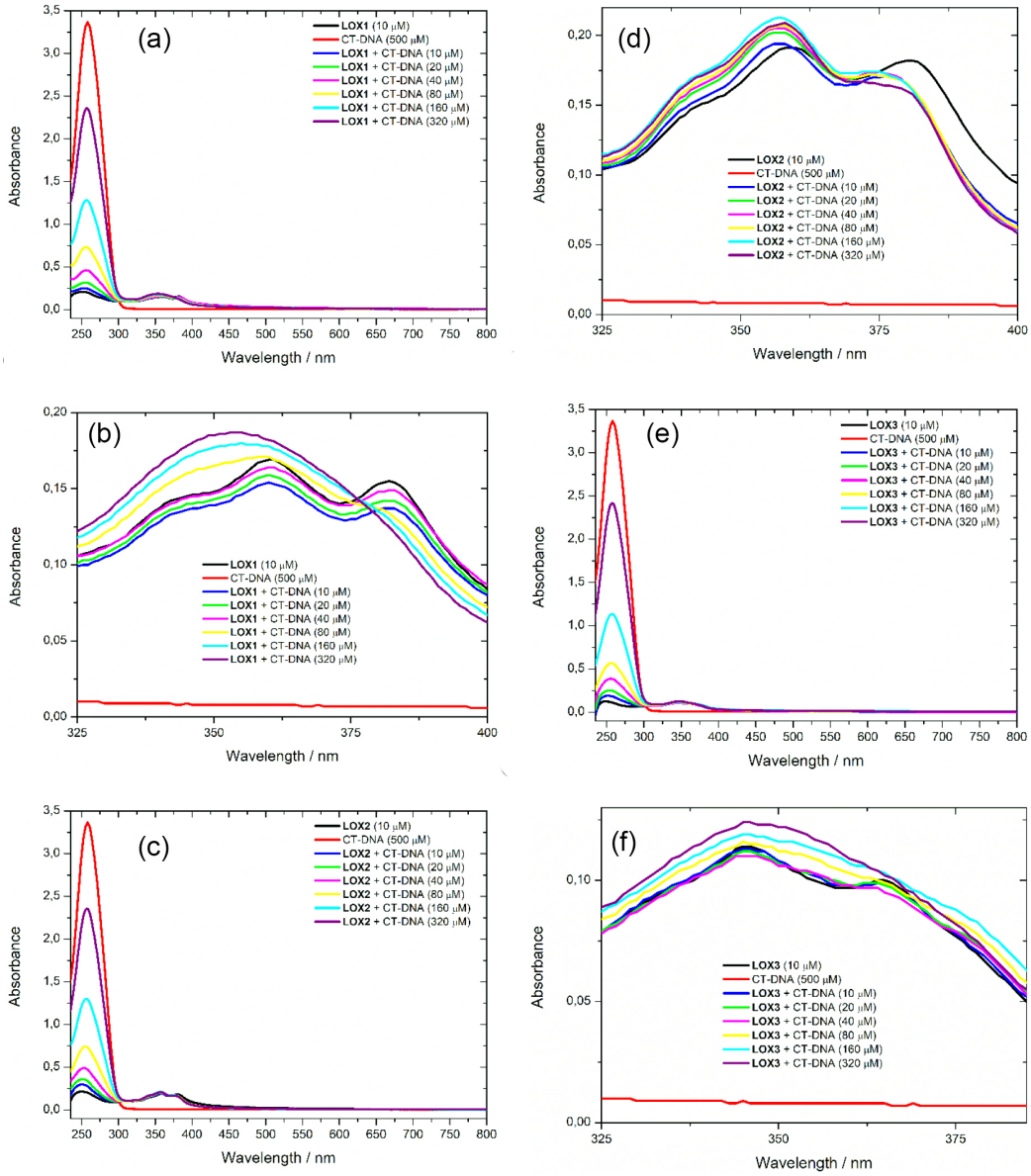


**Figure 7.** Absorption spectra of **LOX1**, **LOX2**, and **LOX3** upon additions of CT-DNA, in DMSO (5%)/Tris-HCl buffer (pH 7.4). (a), (c), and (e) display the full spectrum, and (b), (d), and (f) highlight the main absorption bands in the visible region of **LOX1**, **LOX2**, and **LOX3**, respectively.

of CT-DNA (10-40 μM), indicative of a hypochromic effect (2.95-8.87%). As the of CT-DNA concentration increased from 10 to 40 μM, the extent of hypochromism decreased from 8.87 to 2.95% (Figure 7).

However, at concentrations above 80 μM of CT-DNA, a gradual increase in the absorbance of the main band was observed, indicative of a hyperchromic effect (1.18-10.65%). Additionally, increasing the CT-DNA concentration from 80 to 320 μM resulted in the appearance of a single broad absorption band with a blue shift of 1-6 nm (Figure 7).

Felouat *et al.*[11] observed a variation in the intensity of the bands during the DNA interaction assay for an ESIPT emitter benzoxazole. Initially, the authors noted a gradual increase in the absorbance of the compounds with the addition of the first aliquots of DNA. However, as the increase in DNA concentration, they observed pronounced hypochromism of the main absorption bands of benzoxazole. According to Felouat *et al.*[11] this significant alteration at higher DNA concentrations may be indicative of a second binding mode occurring after the initial mode of interaction.

The absorption profile of **LOX1** at different concentrations of CT-DNA suggests a potential interaction between **LOX1** and DNA via groove binding, given that this compound does not possess charged groups capable of interacting with the phosphate groups of DNA.[10,47,48] This type of interaction is consistent with the molecular structure of **LOX1**, as aromatic rings connected by bonds that allow free rotation facilitate DNA groove binding.[10]

Similar to what was observed for **LOX1**, addition of aliquots CT-DNA (0-320 μM) to **LOX2** resulted in changes in its absorption profile. A gradual increase in the absorbance of the main band (359 nm) was observed after the addition of CT-DNA aliquots (10-320 μM), characteristic of a hyperchromic effect (1.57-11.51%). This hyperchromism was accompanied by a blue shift (1-2 nm) (Figure 7).

It was also noticeable that, at the highest concentration of CT-DNA (320 μM) in the assay, **LOX2** exhibited a smaller blue shift (1 nm) compared to other concentrations. Additionally, at 320 μM of CT-DNA, **LOX2** demonstrated a lower hyperchromism rate compared to the previous CT-DNA concentration (160 μM), indicating the interaction limit threshold between **LOX2** and DNA (Figure 7).

When assessing the effect of increasing DNA concentrations on the absorption spectrum of EB, Waring[51] observed a progressive bathochromic shift of the maximum absorption band (479 nm) towards a limit that, according to the author, represents the spectrum of EB in a fully complexed form. At this limit, EB exhibits the greatest bathochromic shift, but the hypochromism rate is not the highest.[51] Beyond this limit, there appears to be a trend towards an increase in the band intensity compared with the intensity at lower DNA concentrations.

Thus, the hyperchromism and slight blue shift observed suggest a potential interaction between **LOX2** and DNA via grooves binding, as its molecular structure, similar to **LOX1**, also lacks charged groups capable of interacting with the phosphate groups of DNA.[10,47,48,52]

Except for the initial and final absorbance values of the assay, the DNA binding constant (K or $K_b$) of **LOX2** was determined from the plot of [DNA]/($\varepsilon_a - \varepsilon_f$) *versus* [DNA], where [DNA] is the DNA concentration ($M^{-1}$), $\varepsilon_a$ is the apparent molar absorptivity ($M^{-1}$ $cm^{-1}$; corresponding to the ratio of observed absorbance to species concentration), and $\varepsilon_f$ is the free molar absorptivity ($M^{-1}$ $cm^{-1}$) of the chemical species, i.e., in the absence of DNA. The value of $K_b$ was calculated from the ratio of the slope and intercept coefficients (Figure 8).[3,10,21]

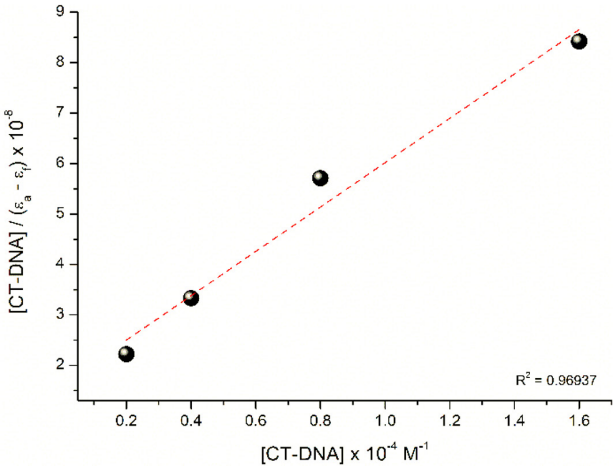


**Figure 8.** Plot of [DNA]/($\varepsilon_a - \varepsilon_f$) *vs.* [DNA] in the main absorption band of the visible region. [**LOX2**] = 10 μM and [CT-DNA] = 20 to 160 μM.

The $K_b$ value of **LOX2** was $2.70 \times 10^4$ $M^{-1}$. This $K_b$ value indicates that **LOX2** can strongly bind to the biomolecule.[50] The DNA binding constant of **LOX2** was higher than the values obtained by Wang *et al.*[2,3] for most of their evaluated naphthoxazoles ($3.58 \times 10^3$-$5.29 \times 10^4$ $M^{-1}$).

In contrast to **LOX1** and **LOX2**, adding of aliquots of CT-DNA (0-320 μM) to **LOX3** has resulted in minor changes in its absorption profile. Initially, a decrease in the absorbance of the main band (346 nm) was observed after the addition of the first aliquots of CT-DNA (10-40 μM), which is characteristic of a hypochromic effect (0.87-3.50%). As the concentration of CT-DNA increased (10 → 40 μM), the rate of hypochromism also increased from 0.87 to 3.50% (Figure 7).

However, similar to what was observed for **LOX1**, a gradual increase in the absorbance of the main band was

noted above 80 μM of CT-DNA, indicating a hyperchromic effect (0.87-8.77%). Additionally, as the concentration of CT-DNA increased from 80 to 320 μM, a single broad absorption band appeared. No significant deviations in the $\lambda_{abs}$ for **LOX3** were observed (Figure 7).

These observations also suggest a potential interaction between **LOX3** and DNA via groove binding, as **LOX3** lacks charged groups that would facilitate binding to the phosphate groups of DNA.[10,47,48] The absence of bathochromic or hypsochromic shifts suggests a weak interaction with the biomolecule.[10,42]

## Conclusions

The naphthoxazoles derived from lapachol (**LOX1**, **LOX2**, and **LOX3**) were synthesized using an economically and environmentally viable synthesis protocol. The range of yields of **LOX1**, **LOX2**, and **LOX3** varied from 19.6 to 43.3%. These compounds exhibited large Stokes shifts, reduced fluorescence, low values of fluorescence quantum yield in their free form, demonstrating behavior similar to that of DAPI. Furthermore, they exhibited typical lifetimes in the nanosecond range. **LOX1** and **LOX3** showed long lifetimes of 14.44 and 8.08 ns, respectively. UV-Vis absorption spectroscopy of DNA binding studies revealed that the naphthoxazoles interact with DNA, as indicated by changes in the absorption properties with increasing concentrations of CT-DNA. The results suggest that **LOX1**, **LOX2**, and **LOX3** bind to DNA via groove binding. Notably, **LOX2** showed a pronounced $K_b$ value, indicating strong binding to DNA. These findings suggest that **LOX1**, **LOX2**, and **LOX3** may be suitable candidates as DNA fluorescent probes.

## Supplementary Information

Supplementary data are available free of charge at http://jbcs.sbq.org.br as PDF file.

## Acknowledgments

The authors would like to thank the FACEPE for financial support IBPG-1482-4.03/19 and APQ-0788-1.06/22, CAPES and the National Laboratory of Bio-Renewables (LNBR) at the National Center for Energy and Materials Research (CNPEM) for the HRMS mass analysis.

### Author Contributions

Délis G. Guimarães was responsible for conceptualization, investigation, data curation, formal analysis, visualization, and writing original draft; Victória L. A. Santos for investigation, writing-review and editing; Sidney S. Simplicio for investigation, writing-review and editing; Arlan A. Gonsalves for formal analysis, resources, writing-review and editing; João J. S. Gouveia for investigation and resources; Fernanda B. Almeida for investigation, data curation and formal analysis; Luiza A. Gusmão for investigation; Antonio C. Tedesco for investigation, data curation; Fernando L. Primo for investigation, data curation, formal analysis and resources; Larissa A. Rolim for funding acquisition and resources; Cleônia R. M. Araújo for conceptualization, data curation, formal analysis, project administration, resources, writing-review and editing.

## References

1. Slovesnova, N. V.; Minin, A. S.; Smolyuk, L. T.; Taniya, O. S.; Tsmokalyuk, A. N.; Kim, G. A.; Kovalev, I. S.; Pozdina, V. A.; Kopchuk, D. S.; Krinochkin, A. P.; Zyryanov, G. V.; Petrov, A. Y.; Charushin, V. N.; *Dyes Pigm.* **2022**, *204*, 110410. [Crossref]
2. Wang, X.-Z.; Yao, J.-H.; Xie, Y.-Y.; Lin, G.-J.; Huang, H.-L.; Liu, Y.-J.; *Inorg. Chem. Commun.* **2013**, *32*, 82. [Crossref]
3. Wang, X.-Z.; Jiang, G.-B.; Xie, Y.-Y.; Liu, Y.-J.; *Spectrochim. Acta, Part A* **2014**, *118*, 448. [Crossref]
4. Zhang, J.; Chen, R.; Zhu, Z.; Adachi, C.; Zhang, X.; Lee, C.-S.; *ACS Appl. Mater. Interfaces* **2015**, *7*, 26266. [Crossref]
5. Santos, V. L. A.; Guimarães, D. G.; Nishimura, R. H. V.; Rolim, L. A.; Gonsalves, A. A.; Araújo, C. R. M.; *Quim. Nova* **2022**, *45*, 560. [Crossref]
6. Bertozo, L. C.; Tutone, M.; Pastrello, B.; da Silva-Filho, L. C.; Culletta, G.; Almerico, A. M.; Ximenes, V. F.; *J. Photochem. Photobiol., A* **2023**, *444*, 114944. [Crossref]
7. Osadchii, S. A.; Shubin, V. G.; Kozlova, L. P.; Varlamenko, V. S.; Filipenko, M. L.; Boyarskikh, U. A.; *Russ. J. Appl. Chem.* **2011**, *84*, 1541. [Crossref]
8. El-din, A. E-D. S.; Abdullah, S.; Sayed, A. E.-D. H.; *Sci. Afr.* **2021**, *13*, e00961. [Crossref]
9. Soriano, E.; Holder, C.; Levitz, A.; Henary, M.; *Molecules* **2016**, *21*, 23. [Crossref]
10. Sirajuddin, M.; Ali, S.; Badshah, A.; *J. Photochem. Photobiol., B* **2013**, *124*, 1. [Crossref]
11. Felouat, A.; Massue, J.; Ulrich, G.; *Dyes Pigm.* **2021**, *185*, 108895. [Crossref]
12. Liu, Q.-Q.; Lu, K.; Zhu, H.-M.; Kong, S.-L.; Yuan, J.-M.; Zhang, G.-H.; Chen, N.-Y.; Gu, C.-X.; Pan, C.-X.; Mo, D.-L.; Su, G.-F.; *Eur. J. Med. Chem.* **2019**, *165*, 293. [Crossref]
13. Deng, C.; Yan, H.; Wang, J.; Liu, B-s.; Liu, K.; Shi, Y-m.; *Arabian J. Chem.* **2022**, *15*, 104242. [Crossref]
14. Santos-Junior, P. F. S.; Nascimento, I. J. S.; da Silva, E. C. D.; Monteiro, K. L. C.; de Freitas, J. D.; de Lima Lins, S.; Maciel, T. M. S.; Cavalcante, B. C.; Neto, J. B. V.; de Abreu,

F. C.; Fegueiredo, I. M.; Santos, J. C. C.; Pessoa, C. Ó.; da Silva-Júnior, E. F.; de Araújo-Júnior, J. X.; de Aquino, T. M.; *New J. Chem.* **2021**, *45*, 13847. [Crossref]
15. Silva, M. M.; Savariz, F. C.; da Silva-Júnior, E. F.; de Aquino, T. M.; Sarragiotto, M. H.; Santos, J. C. C.; Figueiredo, I. M.; *J. Braz. Chem. Soc.* **2016**, *27*, 1558. [Crossref]
16. Santos, V. L. A.; Gonsalves, A. A.; Guimarães, D. G.; Simplicio, S. S.; de Oliveira, H. P.; Ramos, L. P. S.; da Costa, M. P.; de Oliveira, F. C. E.; Pessoa, C.; Araújo, C. R. M.; *Molecules* **2023**, *28*, 3008. [Crossref]
17. de Moura, K. C. G.; Emery, F. S.; Neves-Pinto, C.; Pinto, M. C. F. R.; Dantas, A. P.; Salomão, K.; Castro, S. L.; Pinto, A. V.; *J. Braz. Chem. Soc.* **2001**, *12*, 325. [Crossref]
18. Del Rio, K. P.; de Moura, K. C. G.; Pinto, M. C. F. R.; Leitão, G. G.; *J. Liq. Chromatogr. Relat. Technol.* **2015**, *38*, 1479. [Crossref]
19. Zhang, X.-F.; Zhang, J.; Liu, L.; *J. Fluoresc.* **2014**, *24*, 819. [Crossref]
20. Prajapati, R.; Chatterjee, S.; Kannaujiya, K. K.; Mukherjee, T. K.; *Nanoscale* **2016**, *8*, 13006. [Crossref]
21. Acunha, T. V.; Chaves, O. A.; Iglesias, B. A.; *J. Porphyrins Phthalocyanines* **2021**, *25*, 75. [Crossref]
22. *Microsoft Excel*, Office Home and Student; Microsoft Corporation, Redmond, WA, USA, 2021.
23. Santos, V. L. A.; Gonsalves, A. A.; Araújo, C. R. M.; *Quim. Nova* **2020**, *43*, 1344. [Crossref]
24. Dias, G. G.; Rodrigues, B. L.; Resende, J. M.; Calado, H. D. R.; de Simone, C. A.; Silva, V. H. C.; Neto, B. A. D.; Goulart, M. O. F.; Ferreira, F. R.; Meira, A. S.; Pessoa, C.; Correa, J. R.; da Silva Júnior, E. N.; *Chem. Commun.* **2015**, *51*, 9141. [Crossref]
25. Aljaar, N.; Malakar, C. C.; Conrad, J.; Frey, W.; Beifuss, U.; *J. Org. Chem.* **2013**, *78*, 154. [Crossref]
26. Pavia, D. L.; Lampman, G. M.; Kriz, G. S.; Vyvyan, J. R.; *Introdução à Espectroscopia*, 4th ed.; Cengage Learning: São Paulo, Brazil, 2010.
27. Branco, F. S. C.; Silva, B. V.; do Rio, G. F.; Santana, M. J.; Queiroz Jr., L. H. K.; Pinto, A. C.; Boechat, N.; Lião, L. M.; *Quim. Nova* **2015**, *38*, 1237. [Crossref]
28. Klinhom, N.; Saengsuwan, N.; Sriyab, S.; Prompinit, P.; Hannongbua, S.; Suramitr, S.; *Spectrochim. Acta, Part A* **2019**, *206*, 359. [Crossref]
29. Purkayastha, P.; Chattopadhyay, N.; *J. Mol. Struct.* **2002**, *604*, 87. [Crossref]
30. Khaled, M. M.; Ismail, M. A.; Medien, H. A. A.; Abdel-Shafi, A. A.; Abdel-Samad, H. S.; *Spectrochim. Acta, Part A* **2023**, *288*, 122090. [Crossref]
31. Cao, C.; Cao, C.; *J. Lumin.* **2021**, *239*, 118382. [Crossref]
32. Bureš, F.; *RSC Adv.* **2014**, *4*, 58826. [Crossref]
33. Yin, G.; Li, Y.; Li, S.; Xu, B.; Yang, Q.; Zhang, Y.; Zhao, J.; Cao, X.; *Dyes Pigm.* **2022**, *198*, 110013. [Crossref]
34. Le, B. H.; Nguyen, T.-V. T.; Joo, H. N.; Seo, Y. J.; *Bioorg. Med. Chem.* **2018**, *26*, 4881. [Crossref]
35. Dai, L.; Zhang, Q.; Ma, Q.; Lin, W.; *Coord. Chem. Rev.* **2023**, *489*, 215193. [Crossref]
36. Abeywickrama, C. S.; Wijesinghe, K. J.; Stahelin, R. V.; Pang, Y.; *Sens. Actuators, B* **2019**, *285*, 76. [Crossref]
37. Lakowicz, J. R.; *Principles of Fluorescence Spectroscopy*, 3rd ed.; Springer: New York, USA, 2006.
38. Berezin, M. Y.; Achilefu, S.; *Chem. Rev.* **2010**, *110*, 2641. [Crossref]
39. Nawara, K.; Waluk, J.; *Anal. Chem.* **2017**, *89*, 8650. [Crossref]
40. Eaton, D. F. *Pure Appl. Chem.* **1988**, *60*, 1107. [Crossref]
41. Valeur, B.; *Molecular Fluorescence: Principles and Applications*, 1st ed.; Wiley-VCH Verlag: Weinheim, Federal Republic of Germany, 2001.
42. Lavanya, K.; Babu, P. V.; Bodapati, A. T. S.; Reddy, R. S.; Madku, S. R.; Sahoo, B. K.; *Int. J. Biol. Macromol.* **2023**, *244*, 125301. [Crossref]
43. Ressler, A. J.; Frate, M.; Hontoria, A.; Ream, A.; Timms, E.; Li, H.; Stettler, L. D.; Bollinger, A.; Poor, J. E.; Parra, M. A.; Ma, H.; Seeram, N. P.; Meschwitz, S. M.; Henry, G. E.; *Bioorg. Med. Chem.* **2023**, *90*, 117369. [Crossref]
44. Khan, R.; Tariq, M.; Shaaban, I. A.; Assiri, M. A.; Bhatti, M. H.; Asif, H. M.; *Polyhedron* **2023**, *243*, 116529. [Crossref]
45. Manna, A.; Chakravorti, S.; *J. Phys. Chem. B* **2012**, *116*, 5226. [Crossref]
46. Swathi, M.; Shankar, D. S.; Daravath, S.; Ganji, N.; Lakshmi, P. V. A.; Shivaraj; *Inorg. Chem. Commun.* **2023**, *153*, 110826. [Crossref]
47. Neha, K. N.; *Anal. Biochem.* **2023**, *675*, 115216. [Crossref]
48. Yildiz, U.; Coban, B.; *J. Serb. Chem. Soc.* **2019**, *84*, 563. [Crossref]
49. Wurthner, F.; Kaiser, T. E.; Saha-Moller, C. R.; *Angew. Chem., Int. Ed.* **2011**, *50*, 3376. [Crossref]
50. Tisoco, I.; Köhler, M. H.; Nogara, P. A.; Rocha, J. B. T.; do Nascimento, C. S.; Garcia, R. Q.; De Boni, L.; Iglesias, B. A.; *Inorg. Chim. Acta* **2023**, *556*, 121639. [Crossref]
51. Waring, M. J.; *J. Mol. Biol.* **1965**, *13*, 269. [Crossref]
52. Sahoo, D.; Bhattacharya, P.; Chakravorti, S.; *J. Phys. Chem. B* **2010**, *114*, 2044. [Crossref]

*Submitted: April 9, 2024*
*Published online: September 20, 2024*